

Enhanced properties of Gamma irradiated nano spinels containing cobalt and aluminium ions : Effect of Gamma radiation on structure, electrical, magnetic and thermal stability properties

Emad M. Masoud & Eman S. Abdelazeem

Ionics

International Journal of Ionics The Science and Technology of Ionic Motion

ISSN 0947-7047

Ionics

DOI 10.1007/s11581-018-2676-2



Ionics

International Journal
of Ionics The Science
and Technology of Ionic
Motion

 Springer

 Springer

Your article is protected by copyright and all rights are held exclusively by Springer-Verlag GmbH Germany, part of Springer Nature. This e-offprint is for personal use only and shall not be self-archived in electronic repositories. If you wish to self-archive your article, please use the accepted manuscript version for posting on your own website. You may further deposit the accepted manuscript version in any repository, provided it is only made publicly available 12 months after official publication or later and provided acknowledgement is given to the original source of publication and a link is inserted to the published article on Springer's website. The link must be accompanied by the following text: "The final publication is available at link.springer.com".



Enhanced properties of Gamma irradiated nano spinels containing cobalt and aluminium ions : Effect of Gamma radiation on structure, electrical, magnetic and thermal stability properties

Emad M. Masoud¹ · Eman S. Abdelazeem¹

Received: 8 June 2018 / Revised: 11 July 2018 / Accepted: 30 July 2018

© Springer-Verlag GmbH Germany, part of Springer Nature 2018

Abstract

Unirradiated and irradiated nano spinels ($\text{CoCo}_{0.5}\text{Al}_{1.5}\text{O}_4$, Co_3O_4) were prepared. All investigated samples were characterized using different techniques such as X-ray diffraction (XRD), Fourier-transform infrared (FTIR) analysis, thermal gravimetric analysis (TG), and transmission electron microscope (TEM). XRD and FTIR analyses confirmed the formation of spinel structure in addition to the effect of gamma radiation on the crystalline structure of unirradiated nano spinels. TG analysis showed that the irradiated nano spinels have more thermal stability than unirradiated ones. As an obvious effect of gamma radiation on structure, the irradiated nano spinel sample showed a different particle morphology compared to the unirradiated one. An obvious enhancement of both electrical and magnetic properties was observed for the irradiated nano spinel samples. The irradiated nano spinel sample of cobalt oxide (Co_3O_4) showed the highest AC conductivity value ($2.16 \times 10^{-7} \Omega^{-1} \text{cm}^{-1}$, at room temperature). In contrast, the irradiated nano spinel sample of cobalt aluminate ($\text{CoCo}_{0.5}\text{Al}_{1.5}\text{O}_4$) showed the highest saturation magnetization (M_s) value (2.12 emu g^{-1} , at room temperature). All results were collected and discussed.

Keywords Gamma radiation · Irradiated nano spinels · Magnetic properties · Electrical properties

Introduction

Interest of the scientific community in nanosized materials has increased in recent years due to their unusual physical and chemical properties which are often different from its bulk counterpart. The most remarkable size-dependent properties of magnetic materials are electrical resistivity, saturation magnetization, coercivity, etc. [1]. Also, different methods of nano spinel synthesis [2–8] have been investigated intensively due

to the unique potential applications such as high-density magnetic recording and microwave devices, and magnetic fluids, and also as an absorbent material to remove sulfide gases from hot-coal gas [9, 10]. One example is the cobalt–aluminate material system from which a series of $\text{Co}^{\text{II}}\text{Co}^{\text{III}}\text{Al}_{2-x}\text{O}_4$ spinels (where $x = 0 - 2$) can be derived [11–15], including CoAl_2O_4 , Co_2AlO_4 , and Co_3O_4 . CoAl_2O_4 is well known as Thenard's blue for its impressive optical property and is widely used in the ceramics, glass, and paint industry, and color TV tubes as a contrast-enhancing luminescent pigment [16]. In recent years, a lot of attention have been devoted towards the gamma-irradiation-induced defect creations and modifications in the properties of nanomaterials. Radiation plays a vital role in changing the properties of nanomaterials and the responsible mechanism is still not completely understood. It is generally accepted that radiation have the capability to displace atoms from their lattice site, and this process is responsible for causing changes in the structure of metals. Furthermore, interaction of radiant energy with the matter, especially γ -radiation, is an important problem of researchers from the viewpoint of theory and practice. While passing through the substances, the high-energy electromagnetic radiation such as gamma rays interact with its atomic nuclei or

Highlights

- Unirradiated and irradiated nano spinel samples were prepared.
- Obvious enhancement of both electrical and magnetic properties was observed through a comparison.
- $\text{CoCo}_{0.5}\text{Al}_{1.5}\text{O}_4$ sample showed M_s value of 2.12 emu g^{-1} at room temperature.
- Co_3O_4 sample showed AC conductivity value of $2.16 \times 10^{-7} \Omega^{-1} \text{cm}^{-1}$ at room temperature.

✉ Emad M. Masoud
emad.youssef@fsc.bu.edu.eg; emad_masoud1981@yahoo.com;
<http://www.bu.edu.eg/staff/emadyoussef7>

¹ Chemistry Department, Faculty of Science, Benha University, Benha 13518, Egypt

electrons. These interactions result in an elastic and inelastic scattering of particles attended by the excitation and ionization of the atoms as well as the nuclear reactions and disturbances in the structure of the matter, so-called radiation damage [17]. The investigation of impacts of high-ionizing radiation on semiconducting materials is a great thought for the improvement of radiation-safe materials. Electronic industry obliges materials that experience radiation-impelled scission or cross-connecting for opposite applications while aviation and medicinal applications require exceptionally radiation-stable materials [18]. Gamma rays create an adjustment in the structure and charge carriers' density in a semiconducting material, which modifies the material properties in a commensurable way [19, 20]. This change relies upon the dosage of irradiation and sensibility of the solid materials to specific irradiation [20]. In our present work, we aim to complete our previous work [21] related to nano spinels. In that work, we studied the structural, magnetic, optical, and electrical properties of nano spinel cobalt aluminate prepared using different molar ratios of cobalt: aluminum (Al^{3+} substitution by Co^{2+}), without a dopant, and depending on the ability of cobalt ion to occupy the positions of aluminum in the octahedral sites to compensate for the lack of aluminum to form the cubic spinel structure. The sample containing Co/Al ratio of 1 ($\text{CoCo}_{0.5}\text{Al}_{1.5}\text{O}_4$) showed the best behavior of both electrical and magnetic properties [21]. As a continuation of this work and for the first time, we here try to enhance the magnetic and electrical properties of those spinels, depending on the gamma radiation effect. So, we chose to study two of our previous nano spinel materials; one containing aluminum and the other free of it. These two nano spinels are $\text{CoCo}_{0.5}\text{Al}_{1.5}\text{O}_4$ and Co_3O_4 . We will investigate the effect of gamma radiation on structural, magnetic, optical, and electrical properties of these nano spinels.

Experimental

Synthesis of nano spinels ($\text{CoCo}_{0.5}\text{Al}_{1.5}\text{O}_4$ and Co_3O_4)

$\text{Co}(\text{NO}_3)_2 \cdot 6\text{H}_2\text{O}$ (> 98%, Fluka), $\text{Al}(\text{NO}_3)_3 \cdot 9\text{H}_2\text{O}$ (> 98.5%, Merck), and glycine (> 99.7%, Merck) were used as received without further purification. Appropriate amounts of the starting materials were used (Table 1) to prepare both $\text{CoCo}_{0.5}\text{Al}_{1.5}\text{O}_4$ and Co_3O_4 . All starting materials were introduced with magnetic stirring into 36 ml distilled water. Two kinds of chelated complexes formed with the dissolution of the nitrate salts in the solution. A deep-purple solution was obtained and further heated at 70 °C overnight to remove excess water. During continuous heating, the solution became more and more viscous and finally became a xerogel. The resulting highly viscous xerogel was calcined at 600 °C (at a rate of about 10 °C min^{-1}) for 3 h to finally get cobalt aluminate ($\text{CoCo}_{0.5}\text{Al}_{1.5}\text{O}_4$) and cobalt oxide (Co_3O_4). The two

Table 1 Appropriate amounts of $\text{Co}(\text{NO}_3)_2$, $\text{Al}(\text{NO}_3)_3$, and glycine used for FAS and CAS sample preparation

Sample	$\text{Co}(\text{NO}_3)_2$ (mol)	$\text{Al}(\text{NO}_3)_3$ (mol)	Glycine (mol)
FAS	0.030	0	0.033
CAS	0.150	0.150	0.042

nano spinels were denoted as CAS and FAS for $\text{CoCo}_{0.5}\text{Al}_{1.5}\text{O}_4$ and Co_3O_4 , respectively. Following this, the two samples were irradiated at 40 kGy using Cobalt-60, a radio isotope of Cobalt. Also, the irradiated samples were denoted as ICAS and IFAS for irradiated $\text{CoCo}_{0.5}\text{Al}_{1.5}\text{O}_4$ and Co_3O_4 , respectively.

Characterization of samples

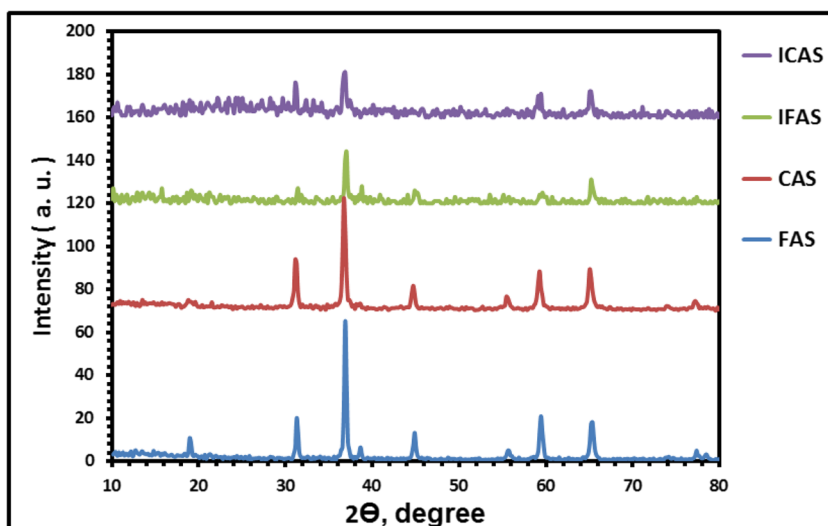
X-ray diffraction analysis was performed on a Diano (made by Diano Corporation, USA). The pattern was run with Cu-filtered $\text{CuK}\alpha$ radiation ($\lambda = 1.5418 \text{ \AA}$) energized at 45 kV, and 10 mA. The samples were measured at room temperature in the range from $2\theta = 10$ to 80° . The infrared spectra of the samples were recorded in the range of 4000–400 cm^{-1} using a Bruker-FT-IR. Thermal analysis (TG) was performed in nitrogen atmosphere with a constant heating rate of 10 K/min in a temperature range of 298–1273 K using Shimadzu DT-50.

The electrical conductivity measurements were performed by sandwiching the powder samples (tablets) between two stainless steel electrodes using a programmable automatic LCR bridge (Model RM 6306 Phillips Bridge) in various temperatures ranging from 298 to 373 K. The UV-Vis spectra were recorded on a UV-visible spectrophotometer (Jasco, model v670). The magnetic properties were measured using vibrating sample magnetometer (VSM; Lake Shore 7404). The morphology was analyzed using a transmission electron microscope (TEM) operating at an accelerating voltage of 200 kV (JEOL, JEM 2100F).

Results and discussion

The XRD patterns of samples are shown in Fig. 1. All irradiated and unirradiated samples exhibited diffraction peaks corresponding to the standard patterns of the spinel (ICSD 01-082-2251). Extremely broad peaks are observed, indicating the presence of very fine particles. No other crystalline phases (like oxides of aluminum) appear in the samples, confirming the purity and also tendency of cobalt ions to compensate for the lack of aluminum ions (Al^{3+}) in the octahedral sites of the spinel that can be fully occupied only by cobalt ions in the FAS sample. As obviously shown, the irradiated samples (ICAS and IFAS) have less intensive peaks and a more amorphous peak nature than the unirradiated ones (CAS and FAS).

Fig. 1 X-ray diffraction patterns of FAS, CAS, IFAS, and ICAS samples



This indicates the obvious effect of gamma radiation on the crystalline structure deformation of spinels. The crystallite size of all samples was calculated using the Scherrer equation [22] and found in a range of 23–25 nm for the unirradiated samples and of 40–62 nm for the irradiated ones (Table 5). As the particle size depends directly on the number of molecules, this also indicates the effect of gamma radiation on the number of molecules per particle.

Figure 2 shows the FT-IR spectra of nano spinels. The band at 3470 cm^{-1} is attributed to the stretching vibrations of the hydrogen-bonded OH groups [23]. The absorption band at 2964 cm^{-1} is related to C–H stretching vibration from the organic compound (glycine) [23]. The characteristics of the stretching bands between 1590 and 1720 cm^{-1} are due to –COOH stretching vibrations [24, 25]. The absorption band at 1097 cm^{-1} is probably due to CH–OH stretching vibration [24]. The bands over the range of 1000 – 400 cm^{-1} ($662, 570\text{ cm}^{-1}$) correspond to metal–oxygen bonds (Co–O and Al–O

stretching) vibrations for the spinel structure compound [23]. The presence of –OH group in all investigated samples is possibly due to the moisture absorption. Additionally, the basic bands of metal oxide of ICAS and IFAS samples showed a slight wave number value shift compared to those of CAS and FAS samples, confirming the effect of gamma radiation on bonding between atoms in the spinel structure.

To further investigate the gamma radiation effect on the morphology, TEM analysis of the $\text{CoCo}_{0.5}\text{Al}_{1.5}\text{O}_4$ sample, as an example, was performed before and after the irradiation process. Figure 3(a, b) shows an obvious difference for the same sample through two scales of magnifications. The unirradiated sample (CAS) showed particles with nanorod agglomeration that was obviously shown through the magnification. As an interesting effect, the irradiated sample (ICAS) showed particles with irregular shape agglomeration that was also shown through the magnification. This indicates the gamma radiation effect in creating defects not only in the atomic

Fig. 2 FT-IR spectra of FAS, CAS, IFAS, and ICAS samples

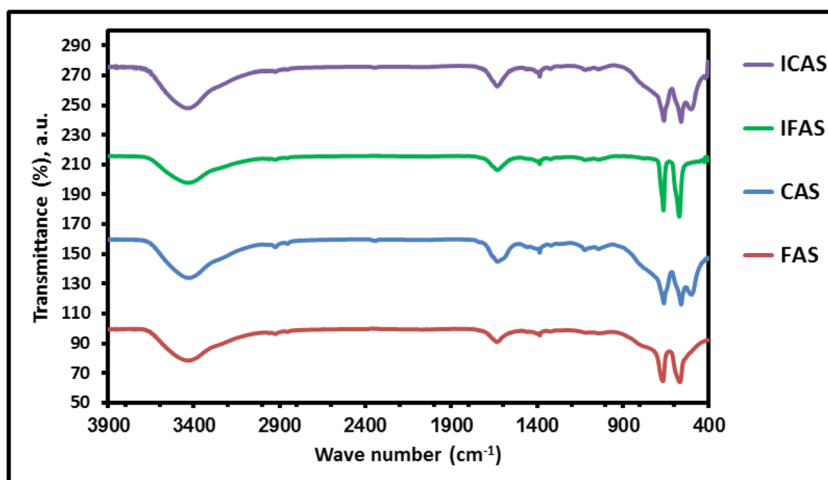
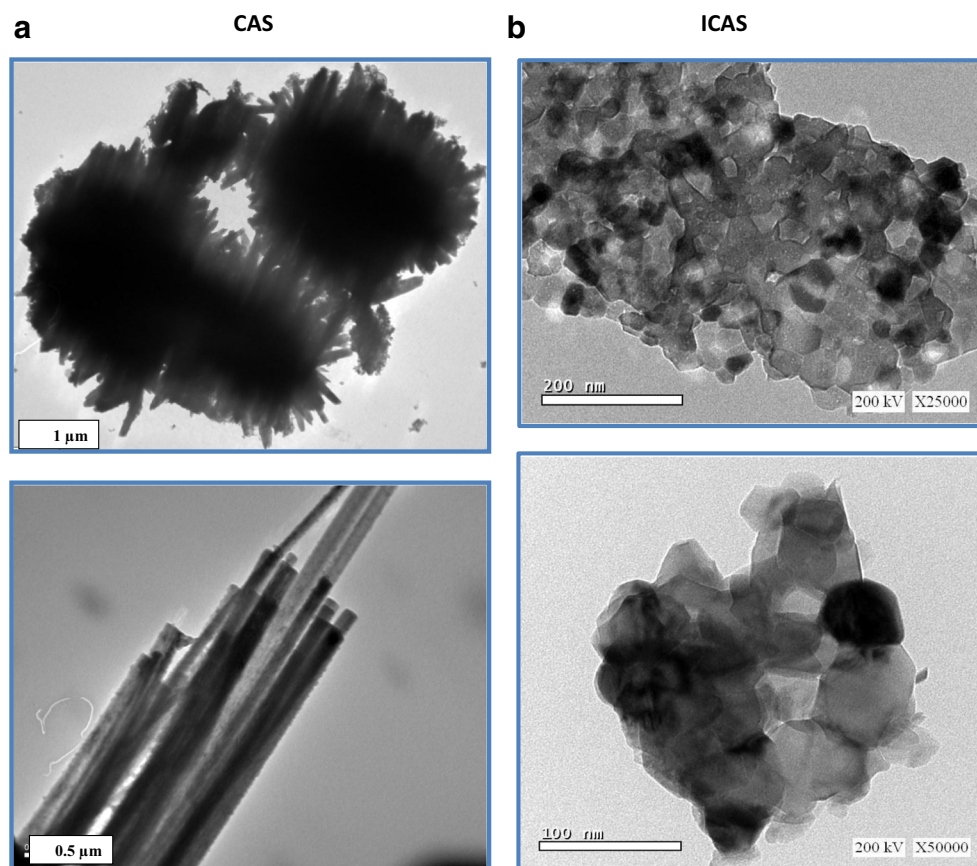


Fig. 3 (a,b) TEM micrographs of CAS and ICAS; with two different magnifications



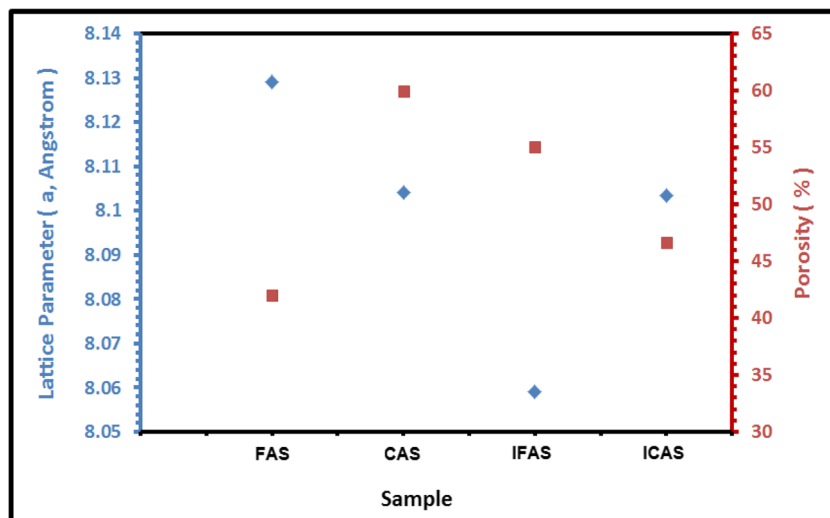
level, but also in the molecular one, and this effect can obviously extend to the particle level. To investigate the gamma radiation effect on the crystal lattice structure, lattice parameter (a), unit cell volume (V), X-ray density (d_x), bulk density (d_b), and porosity parameters were calculated (Table 2 and Fig. 4). The calculated lattice parameter (a) ($a = d_{hkl}(h^2 + k^2 + L^2)^{1/2}$) of unirradiated samples (CAS and FAS) showed that the FAS sample has a higher value than the CAS one. This can be interpreted in light of ionic radius values of both Co^{2+} and Al^{3+} ions. The ionic radius of cobalt (0.745 Å) is larger than that of aluminum (0.535 Å) [26], and as a result, lattice parameter value increases upon substitution. This also demonstrates that the Co- ions actually compensate the lack of Al^{3+} ion concentration and occupy the octahedral sites for

Table 2 Lattice parameter (a), unit cell volume (V), X-ray density (d_x), bulk density (d_b), and porosity of FAS, CAS, IFAS, and ICAS samples

Sample	a (Å)	V (Å ³)	d_x (g/cm ³)	d_b (g/cm ³)	Porosity (%)
FAS	8.129	537.17	5.96	3.42	42
CAS	8.104	532.23	4.81	1.93	60
IFAS	8.059	523.41	6.11	2.74	55
ICAS	8.103	532.09	4.82	2.57	46

all spinel samples [27]. In contrast, the irradiated samples (ICAS and IFAS) showed lower lattice parameter values than the unirradiated ones. This can give an indication of shrinkage of crystal lattice of nano spinels after the gamma irradiation process. This shrinkage may be due to the ability of gamma radiation to convert Co- divalent ions to Co- trivalent ones. As Co- trivalent ion has a lower ionic radius value (0.61 Å) than the Co- divalent one (0.745 Å) [26], this may be the main reason to get low lattice parameter and unit cell volume values of the irradiated samples. Also, the ICAS sample showed the highest lattice parameter value compared to the IFAS one, an opposite trend to that of the unirradiated samples. This also may be attributed to the deformation ratio difference of gamma radiation in the presence of cobalt only or cobalt and aluminum. The X-ray density was calculated using the relation [28]: $d_{x\text{-ray}} = Z \times M/N_A \times V_{\text{cell}}$, where Z is the number of molecules per formula unit (8 for the cubic structure), M is the molar mass, N_A is the Avogadro number (6.02×10^{23} /mol), and V_{cell} is the unit cell volume (Å³). The bulk density was calculated by the following equation [29]: $d_{\text{bulk}} = m/V$ where m is the mass and V ($\pi r^2 h$, where r is the radius and h is the height/thickness of pellet) is the volume of the pellet. The percentage porosity was also calculated using the relation [30]: $P = 1 - d_b/d_x$ where d_b is the bulk density and d_x is the X-ray density. For the unirradiated samples (CAS and

Fig. 4 Lattice parameter (a) and porosity of FAS, CAS, IFAS, and ICAS samples



FAS), the FAS sample showed higher values of bulk and X-ray density than the CAS one. The same behavior was also observed for the irradiated ones. For X-ray density, this may be attributed to the fact that the atomic mass of cobalt (59 amu) is larger than that of aluminum (26.98 amu) [30]. For bulk density, this may be due to the fact that cobalt (8.90 g/cm³) has a larger value of density than aluminum (2.702 g/cm³). These results indicate that the experimental d_b is less than the theoretical d_x and this may be attributed to the presence of pores created during the sintering process [31]. Furthermore, the porosity value of CAS sample is higher than that of FAS one (Fig. 4). This also may be related to the ionic radius difference of cobalt and aluminum ions. Another important notice is that the irradiated samples showed an opposite behavior, where the FAS sample has higher porosity value than the CAS one (Fig. 4). This also shows that gamma radiation effects differ in the presence of cobalt only (FAS), and cobalt and aluminum (CAS).

Figure 5 shows thermal gravimetric analysis (TG) of irradiated and unirradiated samples. Firstly, for unirradiated samples (CAS and FAS), the figure showed weight loss until a temperature of 1000 °C for the CAS sample, but until 850 °C for the FAS one. In general, the weight decrease until 300 °C corresponds to the volatilization of free and adsorbed water molecules. In a region from 300 to 1000 °C, this may be attributed to the decomposition of glycine complexes traces, as confirmed by FT-IR. The glycine complex traces of unirradiated samples were decomposed with a different thermal stability behavior. The FAS sample showed more thermal stability behavior against glycine complex decomposition than the CAS one. This means that the cobalt–glycine complexes are chemically stronger than those of aluminum ones. Secondly, for irradiated samples, the figure showed weight loss until a temperature of 1000 °C for the ICAS sample, but until 925 °C for the IFAS one. On the other hand, the glycine complex traces of irradiated samples were also decomposed with a

Fig. 5 TG analysis of FAS, CAS, IFAS, and ICAS samples

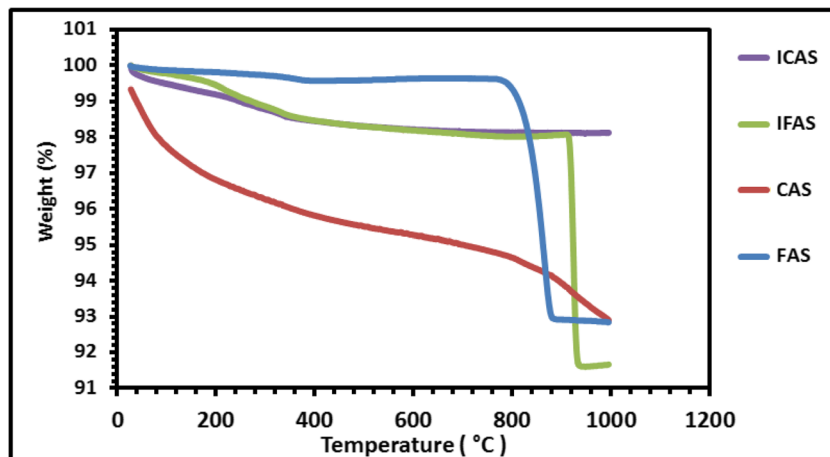
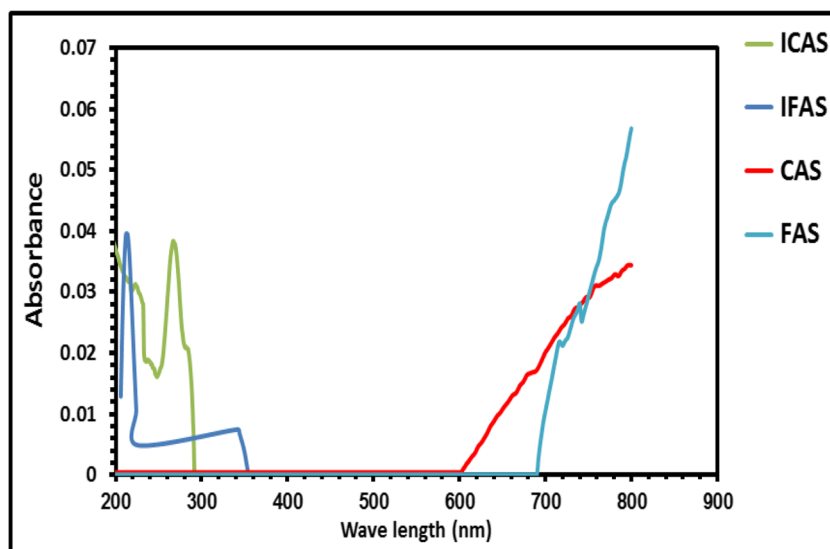


Fig. 6 UV-visible spectra of FAS, CAS, IFAS, and ICAS samples



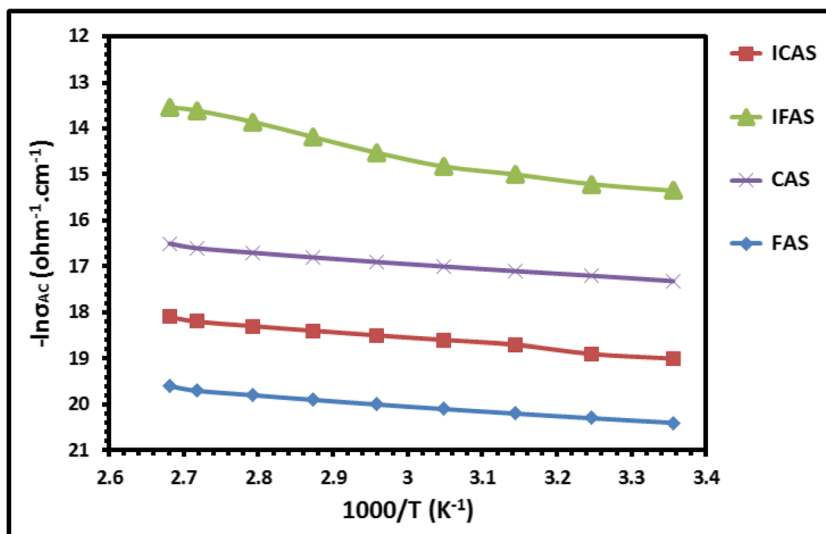
different thermal stability behavior. The IFAS sample showed more thermal stability behavior against glycine complex decomposition than the ICAS one. Also, the figure showed that the irradiated samples have in general more thermal stability behavior than the unirradiated ones. This also shows the gamma radiation destruction and deformation effects on the crystalline structure of nano spinels. The UV-visible spectra of unirradiated and irradiated samples are shown in Fig. 6. For unirradiated samples (CAS and FAS), the figure showed no absorbance at the region between 200 and 600 nm, while an absorbance was observed at the region of 600–800 nm. At the same time, the FAS sample showed an absorbance value higher than that of the CAS one. This demonstrates the effect of aluminum substitution by cobalt and obviously shows electronic transition changes that can take place in the spinel structure. For irradiated samples (ICAS and IFAS), the figure showed an absorbance at the region of 200–350 nm, while no absorbance was observed at the region of more than 350 nm. At the same time, the IFAS sample showed an absorbance value higher than that of the ICAS one. The observed wave number value shift from a region (600–800 nm) to another (200–350) also exhibits the gamma radiation effect of destruction and deformation. All colorimetric parameters (L^* , a^* , and b^*) were determined and tabulated (Table 3). In general, the colorimetric parameters indicate the color, intensity,

and lightness. For unirradiated samples (CAS and FAS), it is obvious that there is a change in all colorimetric parameters, especially the b^* one, which indicates the blue color. The FAS sample showed higher b^* value than that of CAS one. This also confirms the substitution effect of aluminum by cobalt on electronic transitions of nano spinels. These electronic transitions were previously discussed by Zayat and Levy [32], Kim et al. [33], and Stangar UL et al. [34]. On the other hand, for the irradiated samples (ICAS and IFAS), the table showed also higher b^* value of IFAS sample than that of the ICAS one. Moreover, the gamma radiation effect was also confirmed through the value change of all colorimetric parameters (L^* , a^* , and b^*). As obviously shown, all color parameters of IFAS sample are lower than those of FAS one. In contrast, the ICAS sample parameters are higher than those of CAS one. Figure 7 shows the temperature dependence of AC conductivity (at a frequency of 100 Hz) of all investigated samples at a temperature range of 298–373 K. In general, the spinel structure contains defects in the form of Co-, Al-, and O- vacancies [35], which can affect more the electrical properties [36–40], in addition to the expected oxide ion defect formation. These defects produce local structure deformation, in addition to the local displacement in the direction of the local electrical field resulting in the electron hopping. Thus, a number of electrons together with the defects present in the structure form small polarons. So, in addition to electron hopping, the hopping of the small polarons between the adjacent sites, i.e., tetrahedral and/or octahedral sites, occupied by the cobalt or cobalt and aluminum also contributes to the conductivity. Figure 7 showed that AC conductivity values increase with increasing temperature for all investigated samples. This can be mainly attributed to the thermally activated mobility of electrons and that of the small polarons, the hopping of which is enhanced by a rise in temperature. For unirradiated samples, the CAS

Table 3 Colorimetric data of FAS, CAS, IFAS, and ICAS samples

Sample	L^*	a^*	b^*
FAS	16.50	-0.60	-1.27
CAS	16.75	-0.69	-0.48
IFAS	15.48	-0.53	-1.20
ICAS	17.87	-0.70	-0.56

Fig. 7 Temperature dependence of AC conductivity of FAS, CAS, IFAS, and ICAS samples at a frequency of 100 Hz



sample showed a higher conduction value than that of the FAS one. This can be explained in view of the hopping mechanism. This mechanism is considered responsible for the electrical conduction in which the hopping of holes takes place between the interstitial sites to occupy Al³⁺ and cobalt ions (Co²⁺) at the octahedral sites [41]. In contrast, the irradiated samples (ICAS and IFAS) showed an opposite trend compared to those of unirradiated ones. The IFAS sample showed a higher conduction value than that of ICAS. This may be attributed to what was mentioned above, the gamma radiation can induce the formation of Co- trivalent ions, and as a result the IFAS sample will exhibit a higher number of Co- trivalent ions than that of ICAS. This means that the system will have extra electrons, and as a result, the hopping mechanism (between Co²⁺ and Co³⁺ in octahedral) can also be expected.

On the other hand, the gamma radiation effect exhibited an obvious enhancement of the conduction process of FAS sample, but no enhancement was observed for the CAS one. This also may be attributed to the defect formation ratio difference of gamma radiation in the sample of cobalt ions only and that of aluminum and cobalt one, besides the high ratio of Co-trivalent ions existing in the IFAS sample. The IFAS sample showed the highest conduction value of $2.15 \times 10^{-7} \Omega^{-1} \text{ cm}^{-1}$,

at room temperature (Table 4). The other samples showed the following conduction values in the order: [CAS; $\sigma_{AC} = 3 \times 10^{-8} \Omega^{-1} \text{ cm}^{-1} > \text{ICAS}; \sigma_{AC} = 5.6 \times 10^{-9} \Omega^{-1} \text{ cm}^{-1} > \text{FAS}; \sigma_{AC} = 1.38 \times 10^{-9}$], at room temperature.

The temperature dependence of AC conductivity can be described by the Arrhenius formula [42].

$$\sigma_{AC} = \sigma_0 \exp.(-E_{AC}/kT) \tag{1}$$

Where, σ_0 is a temperature-independent term, k is the Boltzman constant, T is the absolute temperature, and E_{AC} is the apparent activation energy. Figure 8 represents the activation energy values. The figure showed that the IFAS sample has the lowest one (0.25 eV) compared to the other ones having the following activation energy values in the order: [CAS; 0.14 eV > ICAS; $\sigma_{AC} = 0.11 \text{ eV} > \text{FAS}; 0.10 \text{ eV}$]. The effect of temperature on both dielectric constant and loss was also studied at 100 Hz for all investigated samples (Figs. 9,

Table 4 Values of conductivity and activation energy of FAS, CAS, IFAS, and ICAS samples

Sample	AC conductivity at 298 K ($\Omega^{-1} \text{ cm}^{-1}$)	Activation energy (E_a , eV)	Bulk conductivity at 298 K ($\Omega^{-1} \text{ cm}^{-1}$)
FAS	1.53×10^{-9}	0.14	7.89×10^{-9}
CAS	3.10×10^{-8}	0.10	3.00×10^{-8}
IFAS	2.16×10^{-7}	0.25	2.14×10^{-7}
ICAS	5.60×10^{-9}	0.11	2.59×10^{-9}

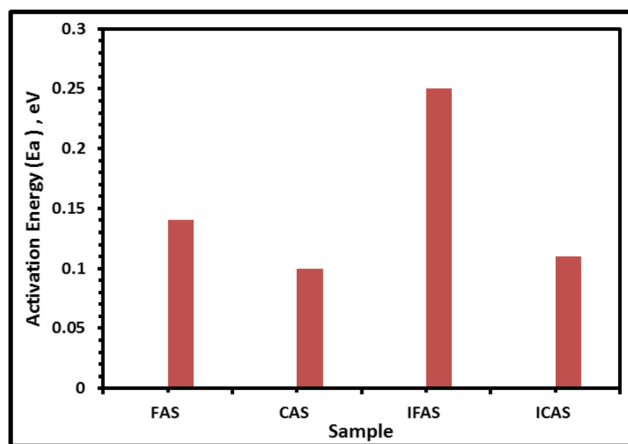
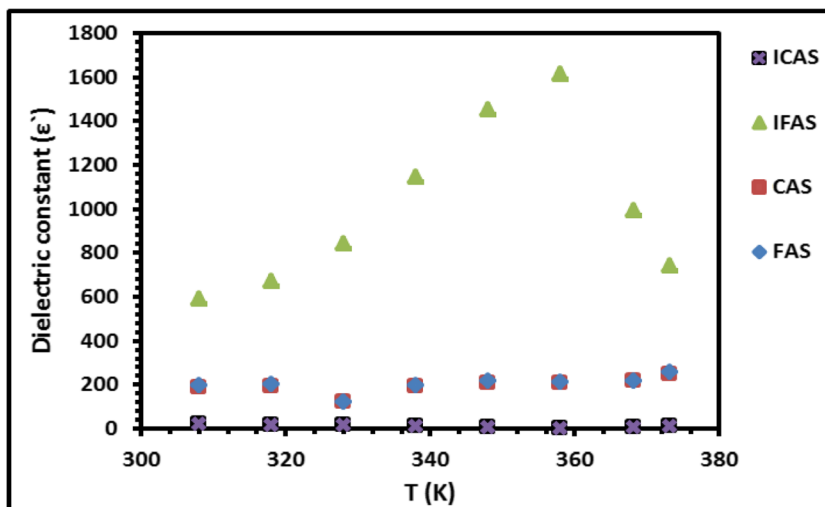


Fig. 8 Activation energy values of FAS, CAS, IFAS, and ICAS samples at a frequency of 100 Hz

Fig. 9 Temperature dependence of dielectric constant (ϵ') of FAS, CAS, IFAS, and ICAS samples at a frequency of 100 Hz



10). For dielectric constant, in general, all samples except the IFAS one exhibited an increase in behavior with increasing temperature. The IFAS sample showed an increase in behavior until a temperature value of around 360 °C, then a decrease was observed until 373 °C. The dielectric constant increase can be interpreted on the basis that as the temperature increases, the thermal energy liberates more electronic transitions and the field tries to align them in its direction [43]. For unirradiated samples, the FAS sample showed a higher dielectric constant value than that of the CAS one. The same thing was also observed for irradiated samples. As observed, the irradiated samples showed higher dielectric constant values than those of the unirradiated ones; this also may be due to the deformation effect or/and different cobalt ion ratios. The IFAS sample showed the highest dielectric constant value (535.2) compared to the other ones that come according to the following order: [FAS; 60.83 > CAS; 50 > ICAS; 28.69], at

room temperature. On the other hand, the dielectric loss behavior comes identical to that of dielectric constant one (Fig. 10). The only difference was that the CAS sample showed higher dielectric loss value than that of the FAS sample. The dielectric loss value increase with increasing temperature may be due to the relaxation of charges in cooperation with the resulting drop in the relaxation time; this, in turn, exerts a double effect on the dielectric loss. On one hand, the friction between the charges will be increased and then the increase in energy dissipation. On the other hand, the energy required to overcome the internal mechanical friction of the medium will be decreased. Also, the IFAS sample showed the highest dielectric loss value (4441) compared to the other ones that come according to the following order: [CAS; 1900 > FAS; 61 > ICAS; 31], at room temperature. To further investigate the electrical properties of all investigated samples, dielectric constant and loss were also studied with different

Fig. 10 Temperature dependence of dielectric loss (ϵ'') of FAS, CAS, IFAS, and ICAS samples at a frequency of 100 Hz

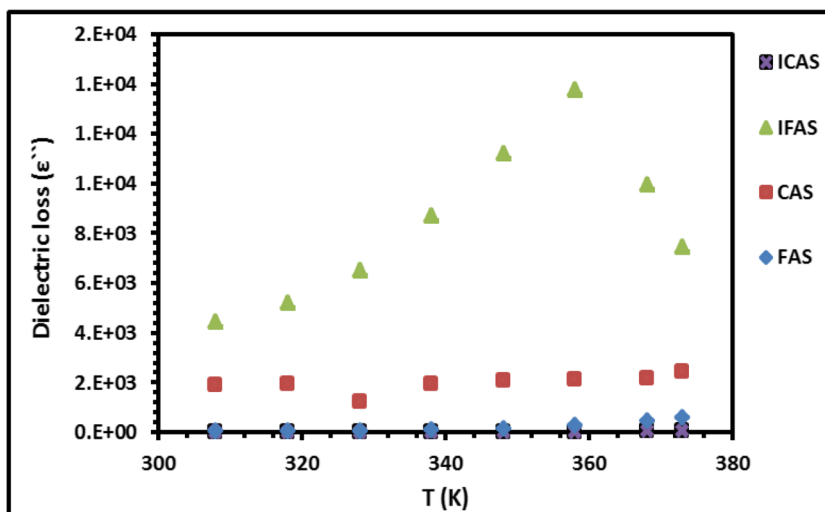
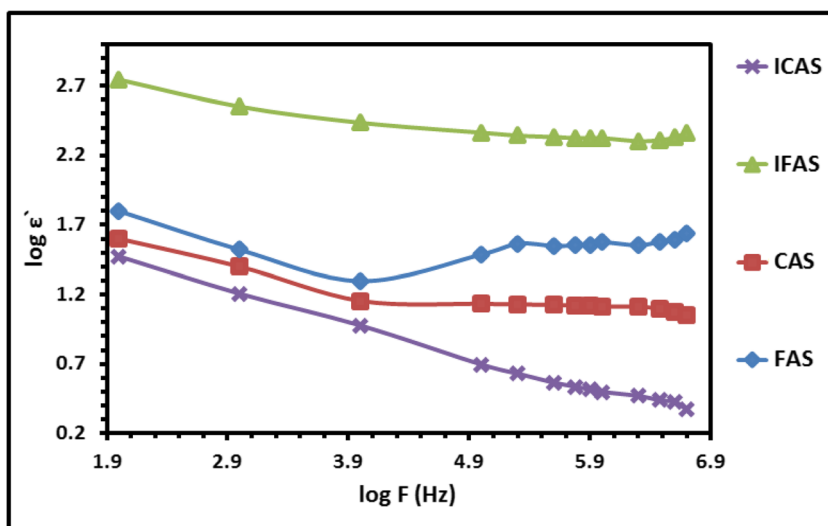


Fig. 11 Frequency dependence of dielectric constant (ϵ') of FAS, CAS, IFAS, and ICAS samples at room temperature (298 K)

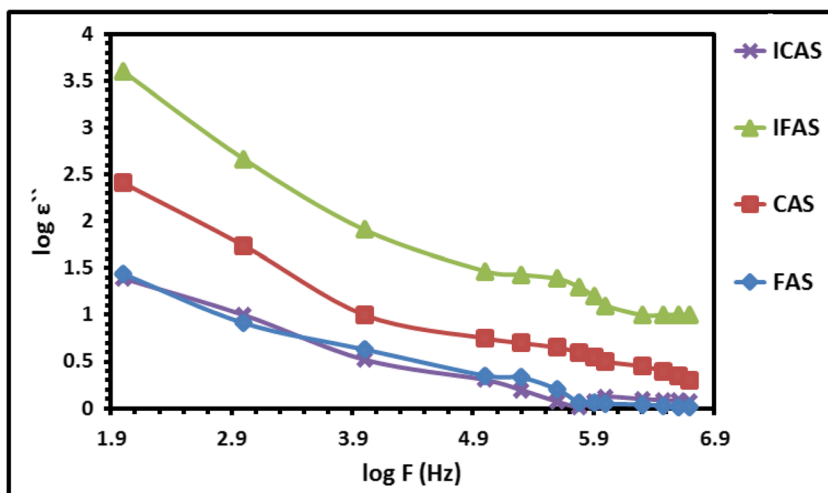


frequencies, at room temperature (298 K) (Figs. 11, 12). The figure exhibited that all samples, in general, have a decrease in behavior of both dielectric constant and loss with frequency. The dielectric loss decrease with increasing frequency is due to the high periodic reversal of the field at the interface. The contribution of charges towards the dielectric loss decreases with increasing frequency. Moreover, all values of dielectric constant and loss at room temperature for both of unirradiated and irradiated samples come in typical arrangement with those at a frequency of 100 Hz. The IFAS sample showed the highest dielectric constant value (554.88) compared to the other ones that come according to the following order: [FAS; 63.07 > CAS; 40 > ICAS; 29.75], at room temperature. The IFAS sample showed the highest dielectric loss value (4001.7) compared to the other ones that come according to the following order: [CAS; 256.63 > FAS; 27.58 > ICAS; 24.63], at room temperature.

To investigate the effect of gamma radiation on bulk conductivity value of all investigated samples, the complex impedance spectra were also studied (Fig. 13). The figure showed an impedance spectrum consists of a semicircle for all samples. This semicircle can be attributed to the electronic conduction process [44–50]. Also, the bulk conductivity values at room temperature were calculated (Table 4). The IFAS sample showed the highest bulk conductivity value of $2.14 \times 10^{-7} \Omega^{-1} \text{ cm}^{-1}$. The other samples showed the following values in the order: [CAS; $\sigma_b = 3 \times 10^{-8} \Omega^{-1} \text{ cm}^{-1}$ > ICAS; $\sigma_b = 5.59 \times 10^{-9} \Omega^{-1} \text{ cm}^{-1}$ > FAS; $\sigma_b = 7.89 \times 10^{-9} \Omega^{-1} \text{ cm}^{-1}$], at room temperature. This arrangement is identical to that of AC conductivity one, as previously discussed. Furthermore, the equivalent circuit was also determined and shown in Fig. 13. Where R1 is the bulk resistance of the sample, and C1 is its bulk capacity.

Figure 14 shows magnetization (M) versus applied magnetic field (H) at room temperature for all investigated

Fig. 12 Frequency dependence of dielectric loss (ϵ'') of FAS, CAS, IFAS, and ICAS samples at room temperature (298 K)



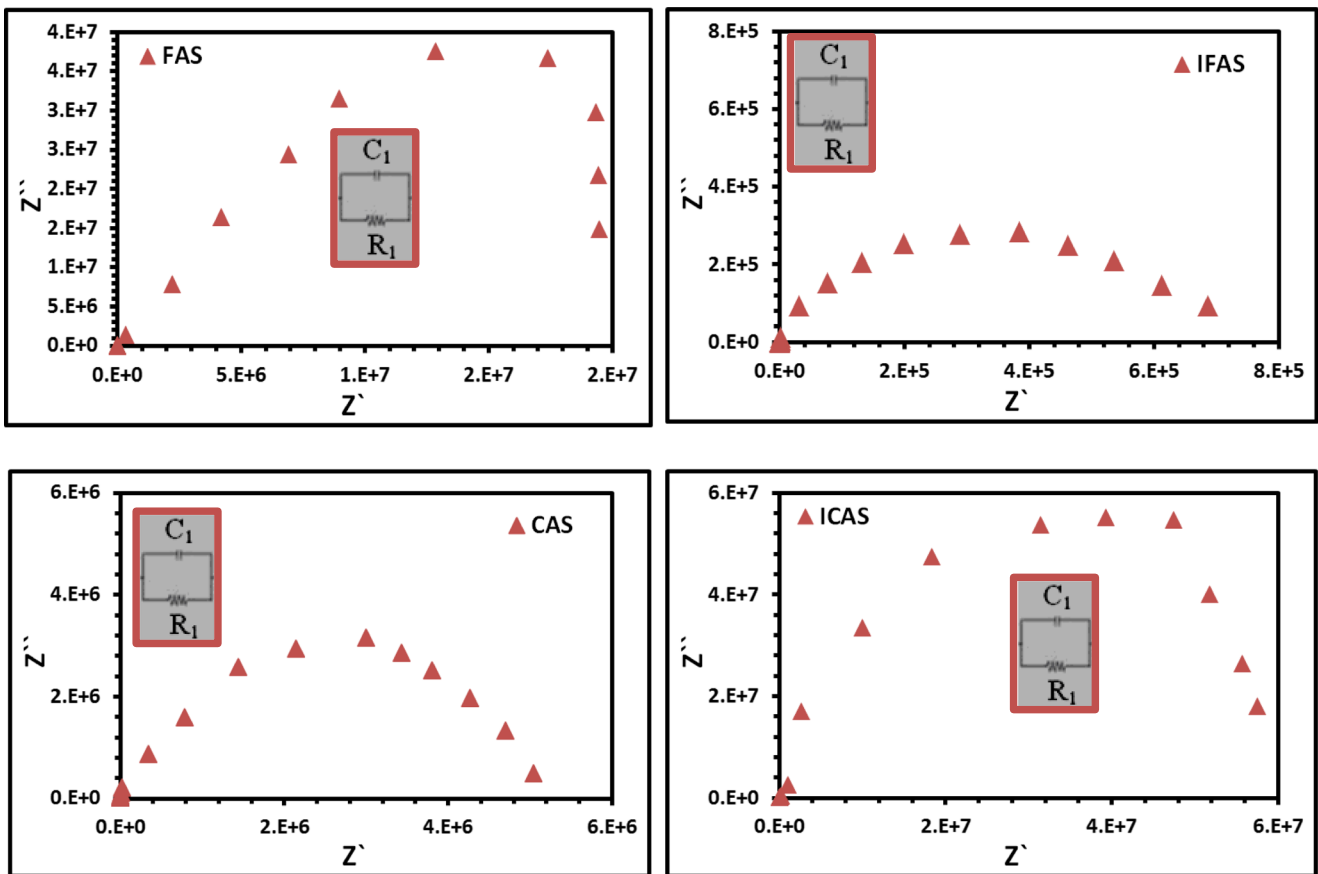


Fig. 13 Complex impedance spectra of FAS, CAS, IFAS, and ICAS samples at room temperature (298 K)

samples. All magnetic parameter values are shown in Table 5. All samples showed absence of hysteresis loop, which indicates the presence of super paramagnetic and single-domain crystals [51]. The little opened loop observed for the ICAS sample may be related to the uncompensated surface spin of the nanoparticles. For unirradiated samples, the CAS sample

showed a higher saturation magnetization value (M_s) than that of the FAS one. This indicates that the spinel containing equal molar ratio of cobalt and aluminum ions represents more enhanced saturation magnetization value than that containing only cobalt ones. This can also be discussed in view of particle size; the same sample showed smaller particle size than that of

Fig. 14 M-H curves of FAS, CAS, IFAS, and ICAS samples at room temperature (298 K)

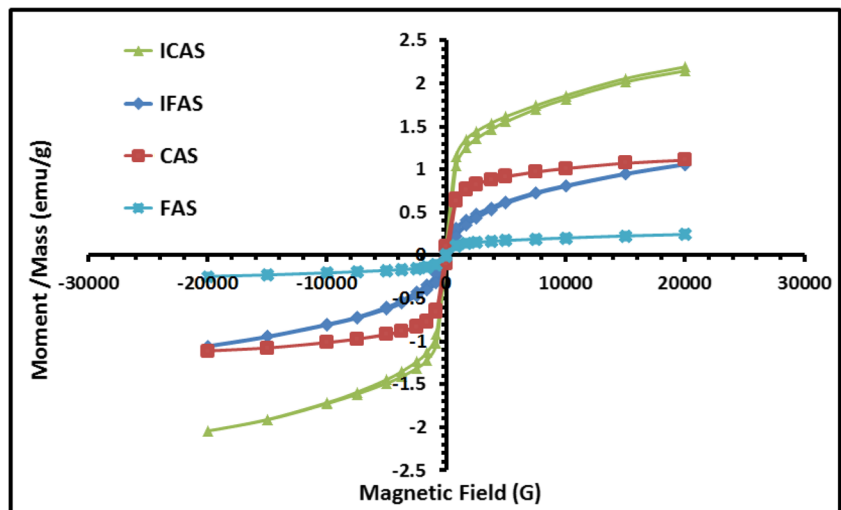


Table 5 Values of particle size, remanent magnetization saturation magnetization (M_s), and coercivity (H_c) of FAS, CAS, IFAS, and ICAS samples

Sample	Particle size (nm)	M_r (emu/g)	M_s (emu/g)	H_c (G)
FAS	25	11.71×10^{-3}	0.243	84.67
CAS	23	98.09×10^{-3}	1.110	112.32
IFAS	62	84.61×10^{-3}	1.058	232.65
ICAS	40	74.19×10^{-3}	2.120	58.30

FAS one (Table 5). This enhancement can be attributed to a modification in the long-range cycloid spin structure of cobalt aluminate spinel [52]. Likewise, the irradiated samples showed that the IFAS sample has a higher M_s value than that of ICAS one, even with the large particle size. Here, it is a worthwhile to mention that the presence of trivalent cobalt ions induced by the gamma radiation, as previously discussed, can affect positively more than the particle size, as trivalent cobalt ion has more magnetic moments than the divalent one [53, 54]. In general, there are two important factors affecting the magnetic properties of the spinel structures: particle size and molar ratio. For our investigated samples, there is a competition between the two factors, at the same time. These two factors can affect with two important mechanisms, surface-driven effect is the enhancement of the magnetic anisotropy (Keff) with decreasing particle size [55, 56]. In addition to the surface effect, the order–disorder characteristic of the samples has also a strong influence on the decrease of saturation magnetization [57]. All saturation magnetization (M_s) values were also represented in Fig. 15. The figure showed that the ICAS sample has the highest saturation magnetization value (M_s), 2.12 emu g^{-1} compared to the other ones, which showed the following values in the order: [CAS; $M_s = 1.11$ emu g^{-1} > IFAS; $M_s = 1.11$ emu g^{-1} > FAS; $M_s = 0.243$ emu g^{-1}], at room temperature.

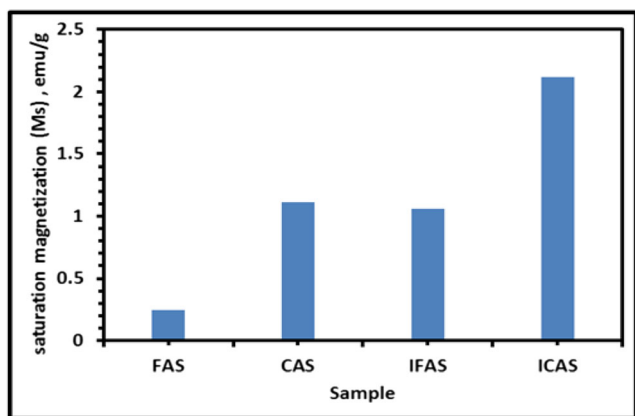


Fig. 15 Saturation magnetization (M_s) values of FAS, CAS, IFAS, and ICAS samples at room temperature (298 K)

Table 6 Comparison of electrical (AC conductivity, $\Omega^{-1} \text{ cm}^{-1}$, at room temperature) and magnetic (M_s , emu g^{-1} , at room temperature) properties of irradiated samples with other recent and previous ones

Sample	Electrical properties (AC conductivity, $\Omega^{-1} \text{ cm}^{-1}$, at room temp.)	Magnetic properties (M_s , emu g^{-1})	Reference
IFAS (irradiated Co_3O_4)	2.16×10^{-7}	1.058	This work
ICAS (irradiated $\text{CoCo}_{0.5}\text{Al}_{1.5}\text{O}_4$)	5.60×10^{-9}	2.120	This work
CoAl_2O_4	–	0.23	[58]
$\text{MgAl}_{0.5}\text{Co}_{1.5}\text{O}_4$	1×10^{-8}	–	[59]
$(\text{Co,Ni})\text{Al}_2\text{O}_4$	5.9×10^{-10}	–	[60]
Co_3O_4	–	0.08	[61]
Co_3O_4	–	0.10	[62]
Co_3O_4	–	0.62	[63]
Co_3O_4	–	0.37	[64]
Co_3O_4	–	0.40	[65]

To further show the enhanced electrical and magnetic properties of our investigated samples, a comparison with other recent previous works was performed (Table 6). The table showed that irradiated samples have obvious enhancement of both electrical and magnetic properties. This indicates that these samples are promising for different applications such as magnetic recording, microwave devices, and magnetic fluids.

Conclusions

Nano spinels ($\text{CoCo}_{0.5}\text{Al}_{1.5}\text{O}_4$ and Co_3O_4) were prepared using the sol–gel method. These samples were irradiated at 40 kGy using Cobalt-60, a radio isotope of cobalt. Structural, electrical, and magnetic properties were investigated for the unirradiated and irradiated samples. X-ray and FT-IR analyses confirmed the spinel structure formation and the effect of gamma radiation on the crystallinity of unirradiated samples. Moreover, different shape morphologies of particles were observed due to the gamma radiation effect. The irradiated samples exhibited in general more thermal stability behavior than the unirradiated ones. The IFAS sample showed the highest conduction value of $2.15 \times 10^{-7} \Omega^{-1} \text{ cm}^{-1}$. The other samples showed the following conduction values in the order: [CAS; $\sigma_{AC} = 3 \times 10^{-8} \Omega^{-1} \text{ cm}^{-1}$ > ICAS; $\sigma_{AC} = 5.6 \times 10^{-9} \Omega^{-1} \text{ cm}^{-1}$ > FAS; $\sigma_{AC} = 1.38 \times 10^{-9} \Omega^{-1} \text{ cm}^{-1}$], at room temperature. Also, the IFAS sample showed the highest dielectric constant value (535.2) compared to the other ones that come according to the following order: [FAS; 60.83 > CAS; 50 > ICAS; 28.69], at room temperature. Additionally, the ICAS sample showed the highest saturation magnetization value (M_s), 2.12 emu g^{-1} , compared to the other ones which exhibited the following values in the order: [CAS;

$M_s = 1.11 \text{ emu g}^{-1} > \text{IFAS}$; $M_s = 1.11 \text{ emu g}^{-1} > \text{FAS}$; $M_s = 0.243 \text{ emu g}^{-1}$, at room temperature. In conclusion, we can state that the IFAS sample exhibited the best electrical properties; and the ICAS one exhibited the best magnetic ones. In a comparison with other previous works, the investigated samples showed an obvious enhancement in both electrical and magnetic properties. This obvious enhancement makes these samples promising candidates for different scientific applications such as magnetic recording, microwave devices, and magnetic fluids.

Funding information The first and corresponding author of this research paper received financial support from Benha University (<http://www.bu.edu.eg/en/>), Egypt, to complete this research work.

References

- Limaye MV, Singh SB, Date SK, Kothari D, Reddy VR, Gupta A, Sathe V, Choudhary J, Kulkarni SK (2009) High coercivity of oleic acid capped CoFe₂O₄ nanoparticles at room temperature. *J Phys Chem B* 113:9070–9076
- Reddy MV, Beichen Z, Jia'en Nicholette L, Kaimeng Z, Chowdari BVR (2011) Molten Salt Synthesis and Its Electrochemical Characterization of Co₃O₄ for Lithium Batteries. *Electrochem Solid-State Lett* 14:A79
- Reddy MV, Kenrick KYH, Wei TY, Chowdar BVR (2011) Nano-ZnCo₂O₄ Material Preparation by Molten Salt Method and Its Electrochemical Properties for Lithium Batteries. *J Electrochem Soc* 158(12):A1423
- Reddy MV, Cai Yu, Fan Jiahuan, Kian Ping Loh and B. V. R. Chowdari, Molten salt synthesis and energy storage studies on CuCo₂O₄ and CuO-Co₃O₄. *RSC Adv* 2(2012)961
- Reddy MV, Xu Y, Rajarajan V, Ouyang T, Chowdari BVR (2015) Template Free Facile Molten Synthesis and Energy Storage Studies on MCo₂O₄ (M = Mg, Mn) as Anode for Li-Ion Batteries. *ACS Sustain Chem Eng* 3(12):3035–3042
- ShahulHameed A, Bahiraei H, Reddy MV, Shoushtari MZ, Vittal JJ, Ong CK, Chowdari BVR (2014) Lithium Storage Properties of Pristine and (Mg, Cu) Codoped ZnFe₂O₄ Nanoparticles. *ACS Appl Mater Interfaces* 6(13):10744
- Darbar D, Reddy MV, Sundarrajan S, Pattabiraman R, Ramakrishna S, Chowdari BVR (2016) Anodic electrochemical performances of MgCo₂O₄ synthesized by oxalate decomposition method and electrospinning technique for Li-ion battery application. *Mater Res Bull* 73:369
- Reddy MV, Quan CY, Teo KW, Ho LJ, Chowdari BVR (2015) Mixed Oxides, (Ni_{1-x}Zn_x)Fe₂O₄ (x = 0, 0.25, 0.5, 0.75, 1): Molten Salt Synthesis, Characterization and Its Lithium-Storage Performance for Lithium Ion Batteries. *J Phys Chem C* 119(9):4709
- Bid S, Pradan SK (2003) Preparation of zinc ferrite by high-energy ball-milling and microstructure characterization by Rietveld's analysis. *Mater Chem Phys* 82:27–37
- Ayala RE, Marsh DW (1991) Characterization and long-range reactivity of zinc ferrite in high-temperature desulfurization processes. *Ind Chem Res* 30:55–60
- O.V. Andrushkova, V.A. Ushakov, V.A. Polubojarov, E.G. Avvakumov, Sibirskii Khim Zh 3 (1992) Effect Of Mechanical Activation On Cobalt Oxides And On Synthesis Of Cobalt Aluminate. *Sibirskii Khimicheskii Zhurnal* 97
- Antolini E, Zhecheva E (1998) Lithiation of spinel cobalt oxide by solid state reaction of Li₂CO₃ and Co₃O₄: an EPR study. *Mater Lett* 35:380–382
- Baydi ME, Poillerat G, Rehspringer JL, Gautier JL, Koenig JF, Chartier P (1994) A sol-gel route for the preparation of Co₃O₄ catalyst for oxygen electrocatalysis in alkaline medium. *J Solid-State Chem* 109:281–288
- Chemlal S, Larbot A, Persin M, Sarrazin J, Sghyar M, Rafiq M (2000) Cobalt spinel CoAl₂O₄ via sol-gel process: elaboration and surface properties. *Mater Res Bull* 35:2515–2523
- Cho WS, Kakihana M (1999) Crystallization of ceramic pigment CoAl₂O₄ nanocrystals from Co–Al metal organic precursor. *J Alloys Compd* 287:87–90
- Buxbaum G (1993) *Industrial inorganic pigments*, 1st edn. VCH, Weinheim, p 85
- Ahmed MA, Ateia E, Salem FM (2007) The effect of Ti⁴⁺ ions and gamma radiation on the structure and electrical properties of Mg ferrite. *J Mater Sci* 42:3651–3660
- Rani NS, Sannappa J, Demappa T, Mahadevaiah D (2013) Gamma radiation induced conductivity control and characterization of structural and thermal properties of hydroxyl propyl methyl cellulose (HPMC) polymer complexed with sodium iodide (NaI). *Adv Appl Sci Res* 4:195–219
- Arshak K, Korostynska O, Harris J, Morris D, Arshak A, Jafer E (2008) Properties of BGO thin films under the influence of gamma radiation. *Thin Solid Films* 516:1493–1498
- Holmes-Siedle AG, Adams L (1993) *Handbook of radiation effects*. Oxford University Press, Oxford, New York
- Masoud EM, EL-Bellihi A-A, Bayoumy WA, Abdelazeem ES (2017) Structural, optical, magnetic, and electrical properties of nanospinel containing different molar ratios of cobalt and aluminum ions. *Ionics* 23:2417–2427
- Mahmoud WE, El-Mallah H (2009) Synthesis and characterization of PVP-capped CdSe nanoparticles embedded in PVA matrix for photovoltaic application. *J Phys D Appl Phys* 42:035502
- J. Chandradass, M. Balasubramanian, Ki Hyeon Kim, *Alloys Compd*, 506 (2010) 395–399, Size effect on the magnetic property of CoAl₂O₄ nanopowders prepared by reverse micelle processing
- Nakamoto K (1986) *Infrared and Raman spectra of inorganic and coordination compounds*. John Wiley & Sons, New York
- Schrader B (ed) (1995) *Infrared Raman spectroscopy: methods and applications*. VCH, Weinheim
- Farag ISA, Ahmad MA, Hammad SM, Moustafa AM (2001) Study of cation distribution in Cu_{0.7}(Zn_{0.3-x}Mg_x)Fe_{1.7}Al_{0.3}O₄ by X-ray diffraction using rietveld method. *Egypt J Solids* 24:215
- Iqbal MJ, Farooq S (2007) Effect of doping of divalent and trivalent metal ions on the structural and electrical properties of magnesium aluminate. *Mater Sci Eng B* 136:140–147
- Hong YS, Ho CM, Hsu HY, Liu CT (2004) Synthesis of nanocrystalline Ba(MnTi)_xFe_{12-2x}O₁₉ powders by the sol-gel combustion method in citrate acid-metal nitrates system (x=0, 0.5, 1.0, 1.5, 2.0). *J Magn Magn Mater* 279:401–410
- Barakat MM, Henaish MA, Olofa SA, Tawfik A (1991) Sintering behaviour of the spinel ferrite system Ni_{0.65}Zn_{0.35}Fe_{2-x}Cu_xO₄. *J Therm Anal Calorim* 37:241–248
- Sattar AA (2004) Physical, Magnetic and Electrical Properties of Ga Substituted Mn-Ferrites. *Egypt J Solids* 27:99
- Ahmed MA, Okasha N, Oaf M, Kershi RM (2007) The role of Mg substitution on the microstructure and magnetic properties of Ba Co Zn W-type hexagonal ferrites. *J Magn Magn Mater* 314:128–134
- Zayat M, Levy D (2000) Blue CoAl₂O₄ particles prepared by the sol-gel and citrate-gel methods. *Chem Mater* 12:2763–2769
- Kim KJ, Kim HK, Park YR, Ahn GY, Kim CS, Park JY (2006) Hyperfine Interactions 169:1363–1369
- Stangar UL, Orel B, Krajnc M (2003) *J Sol-Gel Sci Technol* 26: 771–775
- Gritsyna VT, Afanasyev-Charkin IV, Kobayakov VA (1999) Structure and Electronic States of Defects in Spinel of Different

- Compositions MgO-nAl₂O₃:Me. *J Am Ceram Soc*, 82(12):3365–3373
36. Liu L, Huang Y, Li Y, Wu M, Fang L, Hu C, Wang Y (2012) Oxygen-vacancy-related high-temperature dielectric relaxation and electrical conduction in 0.95K_{0.5}Na_{0.5}NbO₃–0.05BaZrO₃ ceramic. *Physica B* (407):136–139
 37. Li Y, Liang F, Liu L, Huang Y, Hu C (2012) Giant dielectric response and charge compensation of Li- and Co-doped NiO ceramics. *Mater Sci Eng B* 177:673–677
 38. Sun X, Deng J, Liu L, Liu S, Shi D, Fang L, Elouadi B (2016) Dielectric properties of BiAlO₃-modified (Na, K, Li)NbO₃ lead-free ceramics. *Mater Res Bull* 73:437–445
 39. Liu L, Elouadi B (2014) Oxygen vacancy-related dielectric relaxation and electrical conductivity in La-doped Ba(Zr_{0.9}Ti_{0.1})O₃ ceramics. *J Mater Sci Mater Electron* (25):4058–4065
 40. Liu L, Shi D, Fan L, Chen J, Li G, Fang L, Elouadi B (2015) Ferroic properties of Fe-doped and Cu-doped K_{0.45}Na_{0.49}Li_{0.06}NbO₃ ceramics. *J Mater Sci Mater Electron* 26:6592–6598
 41. Keer HV, Bodas MG, Bhaduri A, Biswas AB (1975) Studies on Mn₃O₄ MgAl₂O₄ system. *J Inorg Nucl Chem* 37:1605–1607
 42. Kao KC, Hwang W (1981) *Electrical transport in solid*. Pergamon Press
 43. Emad M. Masoud, A.-A. El-Bellihi, W.A. Bayoumy, M.A. Mousa, *J Alloys Compd* 575 (2013) 223–228, Organic–inorganic composite polymer electrolyte based on PEO–LiClO₄ and nano-Al₂O₃ filler for lithium polymer batteries: Dielectric and transport properties
 44. Emad M. Masoud, Citrated porous gel copolymer electrolyte composite for lithium ion batteries application: An investigation of ionic conduction in an optimized crystalline and porous structure. *Alloys Compd* 651(2015)157–163
 45. Masoud EM, Khairy M, Mousa MA (2013) Electrical properties of fast ion conducting silver based borate glasses: Application in solid battery. *Alloys Compd* 569:150–155
 46. Masoud EM, Mousa MA (2015) Silver-doped silver vanadate glass composite electrolyte: structure and an investigation of electrical properties. *Ionics* 21:1095–1103
 47. ElBellihi AA, Bayoumy WA, Masoud EM, Mousa MA (2012) Preparation, characterizations and conductivity of composite polymer electrolytes based on PEO -LiClO₄ and nano ZnO filler. *Bull Korean Soc* 33(9):2949–2954
 48. Masoud EM, El-Bellihi A-A, Bayoumy WA, Mousa MA (2013) Effect of LiAlO₂ nanoparticle filler concentration on the electrical properties of PEO–LiClO₄ composite. *Mater Res Bull* 48(3):1148–1154
 49. Masoud EM (2016) Nano lithium aluminate filler incorporating gel lithium triflate polymer composite: preparation, characterization and application as an electrolyte in lithium ion batteries. *Polym Test* 56:65–73
 50. Masoud EM, Hassan ME, Wahdaan SE, Elsayed SR, Elsayed SA (2016) Gel P (VdF/HFP) / PVAc / lithium hexafluorophosphate composite electrolyte containing nano ZnO filler for lithium ion batteries application: effect of nano filler concentration on structure, thermal stability and transport properties. *Polym Test* 56:277–286
 51. Upadhyay T, Upadhyay RV, Mehta RV (1997) Characterization of a temperature-sensitive magnetic fluid. *Phys Rev B* 55:5585–5588
 52. Wang J, Neaton JB, Zheng H, Nagarajan V, Ogale SB, Liu B, Viehland D, Vaithyanathan V, Schlom DG, Waghmare UV, Spaldin NA, Rabe KM, Wuttig M, Ramesh R (2003) Epitaxial BiFeO₃ multiferroic thin film heterostructures. *Science* 299:1719–1722
 53. Suard E et al (2000) Charge ordering in the layered Co-based perovskite HoBaCo₂O₅. *Phys Rev J* 61B:R11871
 54. Fauth F et al (2001) Interplay of structural, magnetic and transport properties in the layered Co-based perovskite LnBaCo₂O₅ (Ln = Tb, Dy, Ho). *Eur Phys J* 21B:163
 55. Respaud M, Broto JM, Rakoto H, Fert AR, Thomas L, Barbara B, Verelst M, Snoeck E, Lecante P, Mosset A, Osuna J, Ould Ely T, Amiens C, Chaudret B (1998) *Phys Rev Lett* 57:2925–2935
 56. Bodker F, Morup S, Linderoth S (1994) Surface effects in metallic iron nanoparticles. *Phys Rev Lett* 72:282–285
 57. Kumar S, Singh V, Aggarwal S, Mandal UK, Kotnala RK (2010) Influence of Processing Methodology on Magnetic Behavior of Multicomponent Ferrite Nanocrystals. *J Phys Chem C*. <https://doi.org/10.1021/jp911586d>
 58. Chandradassa J, Balasubramanianb M, Kima KH (2010) Size effect on the magnetic property of CoAl₂O₄ nanopowders prepared by reverse micelle processing. *J Alloys Compd* 506:395–399
 59. Ahmad J, Awan MQ, Mazhar ME, Ashiq MN (2011) Effect of substitution of Co²⁺ ions on the structural and electrical properties of nanosized magnesium aluminate. *Physica B* 406:254–258
 60. Harshit Agarwal, T.P. Yadav, O.N. Srivastava, M.A. Shaz, *Ceram Int* 43 (2017) Dielectric response and alternating current conductivity in (Co,Ni)Al₂O₄ nano-spinel. 16986–16992
 61. Ozkaya T, Baykal A, Toprak MS, Koseog'lu Y, Durmus Z (2009) Reflux synthesis of Co₃O₄ nanoparticles and its magnetic characterization. *J Magn Magn Mater* 321:2145–2149
 62. Nirmallesh Naveen A, Selladurai S (2015) Tailoring structural, optical and magnetic properties of spinel type cobalt oxide (Co₃O₄) by manganese doping. *Physica B* 457:251–262
 63. Bhatt AS, Bhat DK, Tai C-w, Santosha MS (2011) Microwave-assisted synthesis and magnetic studies of cobalt oxide nanoparticles. *Mater Chem Phys* 125:347–350
 64. Meher SK, Ranga Rao G (2011) Effect of Microwave on the Nanowire Morphology, Optical, Magnetic, and Pseudocapacitance Behavior of Co₃O₄. *J Phys Chem C* 115(51):25543–25556
 65. Pal J, Chauhan P (2010) Study of physical properties of cobalt oxide (Co₃O₄) nanocrystals. *Mater Charact* 61:575–579